A Spectral Dissimilarity Constrained Nonnegative Matrix factorization based Cancer Screening Algorithm from Hyperspectral Fluorescence Images

Bo Du[1], Liangpei Zhang[2],
1. School of Computer Science, 2. LISEMARS
Wuhan University
Wuhan, China
e-mail: gunspace@163.com

Dacheng Tao[3], Nan Wang[2], Tao Chen[4]
3. Centre for Quantum Computation and Intelligent Systems
University of Technology
Sydney, Australia
4. Institute of Geophysics and Geomatics,
China University of Geosciences, Wuhan, China

Abstract*—Bioluminescence from living body can help screen cancers without penetrating the inside of living body. Hyperspectral imaging technique is a novel way to obtain physical meaningful signatures, providing very fine spectral resolution, that can be very used in distinguishing different kinds of materials, and have been widely used in remote sensing field. Fluorescence imaging has proved effective in monitoring probable cancer cells. Recent work has made great progress on the hyperspectral fluorescence imaging techniques, which makes the elaborate spectral observation of cancer areas possible. So how to propose the proper hyperspectral image processing methods to handle the hyperspectral medical images is of practical importance. Cancer cells would be distinguishable with normal ones when the living body is injected with fluorescence, which helps organs inside the living body emit lights, and then the signals can be catched by the passive imaging sensor. Spectral unmixing technique in hyperspectral remote sensing has been introduced to detect the probable cancer areas. However, since the cancer areas are small and the normal areas and the cancer ares may not pure pixels so that the predefined endmembers would not available. In this case, the classic blind signals separation methods are applicable. Considering the spectral dissimilarity between cancer and normal cells, a novel spectral dissimilarity constrained based NMF method is proposed in this paper for cancer screening from fluorescence hyperspectral images. Experiments evaluate the performance of variable NMF based method and our proposed spectral dissimilarity based NMF methods: 1) The NMF methods do perform well in detect the cancer areas inside the living body; 2) The spectral dissimilarity constrained NMF present more accurate cancer areas; 3) The spectral dissimilarity constraint presents better performance in different SNR and different purities of the mixing endmembers.

Keywords—component; formatting; style; styling; insert *(key words)*

I. INTRODUCTION

Bioluminescence is a type of chemical luminescence, in which luminescence excitation energy comes from within the organism of enzyme-catalyzed reactions.. The foremost advantage of Bioluminescence is its high sensitivity and it can detect at least 100 labeled cells each time.

Fluorescence imaging uses the exciting lights to increase the energy of fluorophore and then emit the the light with long wavelength, which can be detected by proper procedures. Fluorescence imaging has been used to monitor the growing procedure of brain nerve cells which has the advantages that targets points can be variable and different fluorogenes can be used to label different cells.

Much efforts have been done to combine the advantages of bioluminescence and fluorescence imaging [1, 2]. Actually, multispectral in vivo optical imaging technologies with bioluminescence and fluorescence is drawing great interest in recent years [3, 4, 5]. It employs bioluminescence and fluorescence imaging to obtain useful signals of receptors and has become another important biomedicine. imaging techniques. Compared with the conventional biomedicine imaging techniques, such as ultrasonic, Computed tomography, Magnetic Resonance Imaging, positron emission tomography, it provides more straightforward measurements, much safer performance and lower costs. As a results, much research has been done on it in recent years.

The most significant progress is the imaging techniques. Traditional imaging systems are composed of spectroscopic prism, raster and interferometer. The imaging process is done by push broom or sweep. But the difficulty lie on that filter plate with low band pass is expensive. Novel imaging systems have been proposed to alleviate the problem, including acoustic-optical tunable filter (AOTF) and liquid crystal tunable filter (LCTF) [6, 7, 8]. Novel LCTF based imaging systems have been developed in recent years. Typical one is the Maestro imaging system [8], which can obtain the hyperspectral images, covering the visible to near infrared with fine spectral resolution.

As to the hyperspectral image, it is a powerful way to describe the physical meaning of different materials [9]. Its foremost advantage is that the spectral resolution is very fine and the corresponding spectrum of each different material is

This work was supported in part by the National Natural Science Foundation of China under Grants 61102128, the National Basic Research Program of China (973 Program) under Grant 2012CB719905 and 2011CB707105.

continuous and smooth, showing diagonal features for elaborately separating visually very similar objects. So hyperspectral images provides a new way to analyze the distribution of materials of interest [10]. Classical methods employ the spectral unmixing to do the task. It is assumed that the pixels in the image are composed of limited materials' spectra (called endmembers) and the corresponding abundances. This is the so called linear mixture model (LMM) [11, 12, 13]. There are two ways for spectral unmixing: getting the typical spectra for each material and then the abundances can be obtained by least squares methods with these spectra; unmixing the pixels into the classic spectra and the abundances simultaneously [14, 15, 16].

Since many physically meaningful feature should be nonnegative, especially in the linear models, non-negative matrix factorization (NMF) [12] is proposed. Its basic assumption is that NMF is linearly composed of the two matrix, like the LMM, NMF can decompose a high-dimensional dataset into two nonnegative matrices — one is "basis vectors", the other is "coefficient vectors" [17]. As to hyperspectral unmixing, NMF does not need the pure-pixel existence assumption and can determine all the endmembers signatures and their corresponding abundances simultaneously. So NMF has been of much attention in the field of hyperspectral imagery information extraction [18]. In order to alleviate the local minima problem, much research has introduced auxiliary constraints into basic NMF algorithm.

In hyperspectral unmixing field, according to the properties of the signature and the ground distribution, different constrained algorithms have been developed for spectra unmixing application [19-22].Considering the cancer screening applications, it is said that the cancer cells may have limited number so that their distribution is complex with many mixed pixels in the image and getting the pure endmembers beforehand may be difficult; meanwhile, the normal and the cancer areas may not be so separated both spatially and spectrally. In this case, a novel constraint named "endmembers dissimilarity" is proposed in this paper, which is based on the assumption that cancer endmember and the other endmembers' spectra have a large dissimilarity with each other. To evaluate the efficiency of different auxiliary constraints based on NMF for hyperspectral unmixing, extensive experiments on synthetic data and real hyperspectral medical data have been provided in this paper. Several conclusions are drawn from the experiments results, providing instructive clues for applying these constraints in hyperspectral medical unmixing applications.

Our contribution in this paper can be summarized as: 1) introduce NMF methods into hyperspectral medical image unmixing application and evaluate them. 2) propose an endmembers dissimilarity constraint based NMF approach and the experimental results show NMF based methods do be effective in extracting the cancer information from bioluminescence and fluorescence made hyperspectral images; and the proposed method performs best among all the existing constraints.

The remainder of this paper is organized as follows. Section II presents the linear mixed model and basic NMF model. Section III details different types of NMF methods for hyperspectral unmixing, including our proposed endmember dissimilarity constraint. The experiments on synthetic data and real hyperspectral data are showed in Section IV and V, respectively. Section VI concludes the paper.

II. METHODOLOGY

The LMM assumes that one pixel in the hyperspectral dataset is a linear mixture of p known material signature, called endmember: $\mathrm{A}=[a_1,a_2,...,a_p]$, where a_i is one of the endmember spectra with N dimension. The corresponding proportion is called abundance: $\mathrm{S}=[s_1^{\mathrm{T}},s_2^{\mathrm{T}},...,s_p^{\mathrm{T}}]^T$, where each column s_i^{T} is a M dimension vector, corresponding to ith spectra in A with N dimension. Based on LMM, a hyperspectral image dataset can be expressed as :

$$\mathrm{X}=\mathrm{AS}+\varepsilon \tag{1}$$

where X is a N×M matrix representing the hyperspectral dataset with N bands and M samples, ε is the residual error. According to LMM, the abundance matrix should satisfy the abundance sum to one constraint (ASC) and abundance nonnegative constraints (ANC) simultaneously, i.e., $s_1^{\mathrm{T}}+s_2^{\mathrm{T}}+...+s_p^{\mathrm{T}}=\mathbf{1}^{\mathrm{T}}$ and $s_i^{\mathrm{T}}\geq 0$

Based on the argument that the non-negativity is important in human perception, [23] proposed an algorithm that constructs nonnegative representations of non-negative data or images.

The NMF problem can be stated as follows: Given a nonnegative data matrix $\mathrm{X}\in \mathrm{R}_+^{n\times m}$, find two nonnegative matrix $\mathrm{A}=[a_1,a_2,...,a_p]$ and $\mathrm{S}=[s_1^{\mathrm{T}},s_2^{\mathrm{T}},...,s_p^{\mathrm{T}}]$, where $p<m, p<n$, such that:

$$\mathrm{X}\approx \mathrm{AS} \tag{2}$$

One direct way to find A and S is by constructing a optimal problem, which minimizes the Euclidean distance between X and AS :

$$\min_{\mathrm{A,S}} f(\mathrm{A,S})=\left\|\mathrm{X}-\mathrm{AS}\right\|_{\mathrm{F}} \quad s.t.\mathrm{A}\geq 0,\mathrm{S}\geq 0 \tag{3}$$

Non-negative Matrix Factorization algorithm is usually used to human faces recognition and text documents mining [24], it aims to find two non-negative matrices such that the product approximate to the original matrix. Considering (2), it can also be written to $\mathrm{X}\approx \mathrm{ADD}^{-1}\mathrm{S}$, for any nonnegative invertible matrix *D* whose inverse, *D*-1, is also nonnegative. Therefore, it exits many local minima for the NMF model, so the basic NMF model is a non-convexity problem. To compensate the ununique solution problem, auxiliary constraints on A or S are added to basic NMF model such as manifold constraint [25], [26]. Through auxiliary constraints, the solutions with a desired

property which is corresponding to the auxiliary constraint can be obtained.

Due to the the non-convexity of the basic NMF model, some auxiliary constraints which is conductive to hyperspectral unmixing can be used. Therefore the extend models from (3) is proposed to impove basic NMF model for hyperspectral unmixing:

$$\min_{A\geq 0,\ S\geq 0} G(A,S) = f(A,S) + \lambda_1 g_1(A) + \lambda_2 g_2(S) \tag{4}$$

where $f(A,S)$ is defined by (3), $g_1(A)$ is a function constraining the spectral matrix A which is constructed by the spectral properties and $g_2(S)$ is a function constraining the abundance matrix S which represents the ground objects' distribution properties.

A convergence solution can be obtained through an optimizing problem (4) using gradient descent algorithm:

$$S \leftarrow S - \mu_S \nabla_S G(\mathrm{A,S}) \tag{5}$$

$$A \leftarrow A - \mu_A \nabla_A G(\mathrm{A,S}) \tag{6}$$

Alternative iteration with (5) an (6) provides the elemental operation in the optimization problem. Each iteration proceeds towards to the non-increasing direction. Different applications determine different constraints. For hyperspectral unmixing, what we want to perserve is the physically meaning of both the endmembers' spectra and the abundance distribution. Based on this point, several constraints were proposed.

A. 1. Minimum volume constraint (MVC) [18-23]

One effect way to represent hyperspectral image dataset is by a simplex, typical methods include some endmember extraction methods. The basic theory is that hyperspectral dataset can be considered to be enclosed by a simplex whose vertexes correspond to the endmember spectra. All the pixels in a hyperspectral image form a simplex, and the vertices of a convex simplex will be the endmembers of the image. In two-dimensional space (shown in fig. 1), two bands and three endmembers for example, A, B, and C represent the endmembers, and P is a mixed pixel. In theory, all the pixels would lie inside the simplex, so that each can be linearly represented by all the vertexes.

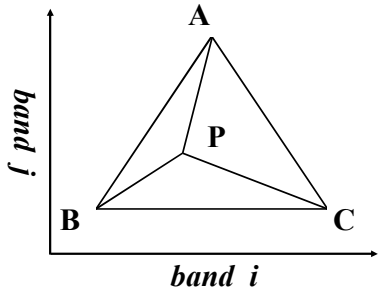

Figure 1. Geometric illustration of each abundances in two-dimensional space

The volume constraint can be written as:

$$g_1(A) = \frac{1}{2(P-1)!}\det^2\left(\begin{bmatrix} 1_P^T \\ A \end{bmatrix}\right)$$
$$\tilde{A} = U^T(A - 1_P^T) \tag{7}$$

The volume constraint has been successfully applied in N-Findr [9] and SGA [10], which find the maximum volume of the dataset. However, these approaches need the assumption that the pure pixel exits in the image. To avoid this , Miao used this volume constraint to NMF by minimizing the volume in order to find a simplex enclosing clean dataset without noise. Through imposing the simplex volume constraint on NMF, one can reconstruct the simplex which corresponds to reality better. Miao's minimum volume constraint as the volume constraint is discussed in this paper.

B. Minimum dispersion constraint (MDC)

Due to the high spectrum resolution, hyperspectral images would present a continuous spectral shape for different land objects. Considering this feature, constrains are proposed to impose the estimated spectra to be flat. Peaks and sharp variations of the spectra curves, or the spectral singularities, are to be preserved. Typical constraint as this kind is minimum dispersion constraint [19], which adds the minimum variances of endmember spectra to the basic NMF model. The minimum dispersion constraint based NMF (MDC NMF) uses variance of the spectral matrix to constrain the recovered spectra to be flat, so as to preserve the possible spectral singularities, mainly the peaks and sharp variations. The minimum dispersion constraint can be written as:

$$g_1(A) = \mathrm{Tr}(\mathrm{A^T A}) - \frac{1}{L}\mathrm{Tr}(\mathrm{A^T 1_{LL} A})$$
$$1_{\mathrm{LL}} = \begin{bmatrix} 1 \ldots 1 \\ 1 \ldots 1 \end{bmatrix}_{L\times L} \tag{8}$$

C. Abundance sparseness constraint (ASC)

In hyperspectral images, it is common that different pixels may not contain all the land objects in the image. So, the abundance distribution of each endmember may not spread all over the scene, implying that for each endmember, its abundance would have a high degree of sparseness [21]. In mathematics, most elements in S are zeros. As to the hyperspectral unmixing, two approaches are used to produce the sparse abundances. One is introducing a smooth matrix C to the NMF algorithm and the update rule is replaced by:

$$S \leftarrow S - \mu_S \nabla_S f(\mathrm{A,S})$$
$$\nabla_S f(\mathrm{A,S}) = \mathrm{AC^T(ACS - X)}$$
$$\mathrm{C} = (1-\theta)\mathrm{I} + \frac{\theta}{P}\mathrm{11^T} \tag{9}$$

where θ between 0 and 1 controls the sparseness of the model. Due to the model, strong smoothing in C will force strong sparseness in both M and S .The other is to project the estimated abundance vector to the desired sparseness. the details of the projection can be found in [27]. The latter method is different from the former one: the former estimates the abundance matrix S through updating the model with smoothing matrix C directly and the latter first estimates the abundance matrix S' from the basic NMF model, then project each vector in the abundance matrix S' to the vector with the desired sparseness. The experimental result shows the former method is faster and higher accuracy in abundance estimation than the latter one,. Therefore, in this paper, the former approach is applied to produce sparse abundance as the abundance sparse constraint.

D. Endmember dissimilarity constraint (EDC)

In this paper, a new spectral constraint named endmember dissimilarity is proposed. For hyperspectral images, even visually similar materials present a distinguishable spectral difference. This point is very vital in sub-pixel mapping or classification analysis. The endmembers are assumed to be the elements composing the mixed pixels, so each should be irreplaceable. This corresponds to the reality. In scene, different ground objects distribute on different areas and present a comparatively large spectral difference. In other words, the introduction of a dissimilarity constraint to NMF frame is promising to enhance the endmember generation, when the basic elemental endmembers are desirable. This thesis proposes an approach aiming at searching a set of vectors with the least similarity so as to find the optimal solution to basic NMF as well as to improve the physical meaning of the resulting endmembers. Mathematically, the ED constraint can be defined as follows:

$$g_1(A)=\sum_{i=1}^{P-1}\sum_{j=i+1}^{P}\mathrm{D}(q_i,q_j)$$

$$\mathrm{D}(q_i,q_j)=\sum_{k=1}^{N}q_{ki}\log\frac{q_{ki}}{q_{kj}}+q_{kj}\log\frac{q_{kj}}{q_{ki}} \qquad (10)$$

$$q_{lc}=\frac{a_{lc}}{T_c},\quad T_c=\sum_{k=1}^{N}a_{kc}$$

where A is the endmember matrix. P is the number of enmembers. N is the band number. a_{ij} is the element in endmember matrix A, $\mathrm{D}(q_i,q_j)$ is the spectral information divergence [28] measuring the similarity between two spectra. The value of $\mathrm{D}(q_i,q_j)$ is 0 if the two spectra are completely same. Therefore, the larger the value of $\mathrm{D}(q_i,q_j)$ is, the more dissimilar between the spectra is.

We introduce this ED constraint into the basic NMF to propose a new model, similar to (7). To obtain an optimization solution to the problem, gradient descent algorithm is employed:

$$S\leftarrow S-\mu_S\nabla_S f(\mathrm{A},\mathrm{S}) \qquad (11)$$

$$A\leftarrow A-\mu_A\nabla_A f(\mathrm{A},\mathrm{S})+\mu_A\lambda_1\nabla_A g_1(\mathrm{A}) \qquad (12)$$

where the derivative of $g_1(A)$ underlying the ED constraint is as follows:

$$\frac{\partial g_1(A)}{\partial a_{uv}}=\sum_{\substack{j=1\\j\neq v}}^{P}[\frac{1-q_{uv}}{T_v}(1+\log\frac{q_{uv}}{q_{uj}})+\frac{1}{T_v}(q_{uj}-\frac{q_{uj}}{q_{uv}})]+$$

$$\sum_{\substack{j=1\\j\neq v}}^{P}\sum_{\substack{k=1\\k\neq u}}^{N}[\frac{-q_{kv}}{T_v}(1+\log\frac{q_{kv}}{q_{kj}})+\frac{q_{kj}}{T_v}]$$

$$=\frac{1}{T_v}\left\{\begin{array}{l}\sum_{j=1}^{P}[(1-q_{uv})(1+\log\frac{q_{uv}}{q_{uj}})+(q_{uj}-\frac{q_{uj}}{q_{uv}})]+\\ \sum_{j=1}^{P}\sum_{\substack{k=1\\k\neq u}}^{N}[-q_{kv}(1+\log\frac{q_{kv}}{q_{kj}})+q_{kj}]\end{array}\right\} \qquad (13)$$

III. EXPERIMENTS AND ANALYSIS

In order to evaluate our proposed method, NMF with different constraints will be evaluated first by the synthetic data and then the real hyperspectral fluorescence dataset containing a cancer rat. All the different constraints mentioned above, including our proposed one, are used.

Two criteria spectral angel distance (SAD)[11] and root mean square error (RMSE) [29] are used to evaluate the unmixing results. This two criteria measure the similarity between the estimated results and the reference values. SAD is defined as :

$$SAD=\cos^{-1}\frac{a_i^T\cdot\hat{a}_i}{|a_i^T||\hat{a}_i|} \qquad (14)$$

where a_i is an estimated endmember signature and $\hat{a}_i$ is the corresponding reference signature.

RMSE measures similarity between the estimated abundance and the corresponding reference abundance, which is defined as:

$$RMSE=\sqrt{\frac{1}{N}\sum_{j=1}^{N}(S_{kj}-\hat{S}_{kj})^2} \qquad (15)$$

where S_{kj} is the estimated abundance and S_{kj} is the corresponding reference abundance.

A. Simulated dataset experiments

The spectral signatures in the synthetic data are chosen from the United States Geological Survey (USGS) digital

spectral library [10]. Fig. 2(a) shows the three endmember signatures used in the experiments. The generation of abundances is similar to that in [22], which takes 3 steps: 1) Five endmembers distribute at the four corners and the center in a 100 × 100 scene, respectively; 2) each endmember diffuses outward, with abundance decreasing until zero; 3) normalize the abundances in order to satisfy abundance sum to 1 constraint. 4) determine the noise signals under different signal to noise ratio (SNR); 5) synthesize the dataset by the endmembers and the corresponding abundances and noise. Fig. 2 (b) shows the abundances of the five endmembers. The noise in the synthetic data is Gaussian noise and the SNR is defined as [30, 31]:

$$SNR = 10\log_{10}\frac{E[x^T x]}{E[n^T n]} \tag{16}$$

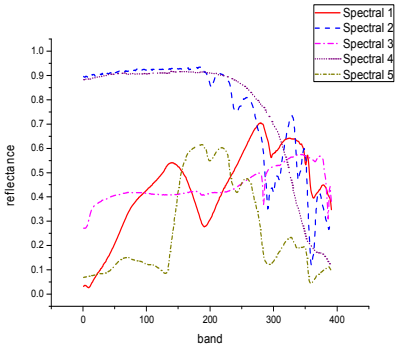

(a)

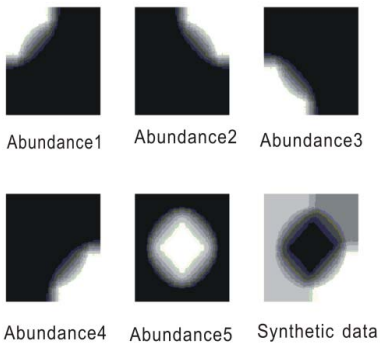

(b)

Figure 2. Example of the synthetic data (a) enmember spectral (b) abundance maps and the 300th band of the synthetic data

Two experiments are conducted to evaluate the effectiveness of NMF with different constraints. In the first experiment, the robustness with respect to different SNR is used to evaluate the constraints. Noise in the hyperspectral images is the main obstacle in spectra unmixing. In order to evaluate the performances of the proposed method under different levels of noises, the Gaussian white noise is implanted into the synthetic dataset with different signal to noise rate. Six different levels of the noise are implanted, including 10 dB, 15 dB, 20 dB, 25 dB, and 30 dB, resulting in six corresponding synthetic datasets.

In the second experiment, the constraints are evaluated by the robustness with different mixing degree which is denoted by purity. The purity is 1 if the pure pixels exist in the scene and it decreases with the increasing mixing degree. And the SNR is fixed as 30 dB. The five different purities are also used to evaluate the performances under different mixing degree: 1, 0.9, 0.8, 0.7, 0.6, 0.5.

The experimental results are quantitatively analyzed by spectral angle measure (SAM) and root mean square error (RMSE) in Table I. and Table II., respectively. SAM presents the accuracy of the generated endmember spectra compared with the reference spectra. SAM with a lower value corresponds to the better endmember. From Table I., it is obvious that at most cases our proposed method presents smallest SAM at most cases, even with a SNR of 10 dB. In other words, our proposed method is insensitive to the varying noise levels. The spectral dissimilarity constraint is superior to other constraint in suppressing the noise in NMF based spectra unmixing. From Table II., the abundances results by our method are also very accurate so that the corresponding RMSE is smallest at all the cases. In a word, our proposed method also comes out better abundances which provides a direct way to determine the distribution of different endmembers.

TABLE I. SPECTRAL ANGLE MEASURE UNDER DIFFERENT SNRS

SNR	10 dB	15 dB	20 dB	25 dB	30 dB	35dB
Proposed	**0.09037**	0.04870	**0.02167**	**0.00875**	**0.00406**	**0.00203**
MDCNMF	0.09991	0.04834	0.02193	0.009076	0.004289	0.00217
MVCNMF	0.09316	**0.04254**	0.0832	0.01042	0.00581	0.00258
ASC NMF	0.10319	0.07382	0.05691	0.04712	0.04120	0.03806

TABLE II. RMSE UNDER DIFFERENT SNR

SNR	10 dB	15 dB	20 dB	25dB	30dB	35dB
Proposed	**0.16500**	**0.10991**	**0.05804**	**0.02473**	**0.01143**	**0.00698**
MDCNMF	0.16580	0.11160	0.05859	0.02539	0.01278	0.00734
MVCNMF	0.27820	0.24614	0.13771	0.02791	0.01344	0.01646
ASC NMF	0.39831	0.44022	0.46922	0.48630	0.49496	0.49864

Another important factor affecting the endmembers' abundance distribution is the mixing degree. With different mixing degrees, a more robust method should present a steady superiority in inversing the abundances. In our experiments, these above mentioned constraints are evaluated by the robustness to different degrees of mixing, which is measured by purity. The purity is 1 if pure pixels exist in the scene, and it decreases with the increasing degree of mixing. For example, we obtained the data with purity equal to 0.8 by removing the pixel of which the abundance is larger than 0.8. Table III. and Table IV. present the SAM and the RMSE . From Table III., it is shown that our proposed method obtain best endmembers

spectra at a purity of 1, 0.9 and 0.8. As the purity continues to reduce, MVCNMF performs best. However, our proposed method presents very similar SAM to that of MVCNMF, with all the other methods revealing a much larger SAM. With regard to Table IV. , it is more obvious that our proposed method keeps least RMSE in all the cases. Since RMSE is a direct way to measure the inversed abundances, it can be safe to conclude that ours proves a convincing and effectual way to determine the exact distribution of the endmembers of interest from mixed signals in HSI datasets.

TABLE III. TABLE III. SPECTRAL ANGLE MEASURE UNDER DIFFERENT PURITIES

Purity	1	0.9	0.8	0.7	0.6	0.5
Proposed	**0.00112**	**0.00911**	**0.02246**	0.04578	**0.07693**	0.17356
MDCNMF	0.10420	0.00920	0.02987	0.04722	0.08741	0.23058
MVCNMF	0.00182	0.00934	0.02451	**0.04525**	0.07909	**0.16598**
ASC NMF	0.02252	0.05061	0.08386	0.11900	0.16084	0.19217

TABLE IV. TABLE IV. RMSE UNDER DIFFERENT PURITIES

Purity	1	0.9	0.8	0.7	0.6	0.5
Proposed	**0.00175**	***0.01779***	***0.0373***	***0.05082***	***0.08147***	***0.13017***
MDCNMF	0.10780	0.11620	0.0955	0.12750	0.15441	0.16310
MVCNMF	0.10681	0.01819	0.03743	0.05701	0.09074	0.14383
ASCNMF	0.44491	0.41905	0.39122	0.34262	0.31431	0.31130

B. Real dataset experiments

This section uses the hyperspectral fluoroscopic images for evaluation of our proposed method. The image dataset acquired by Maestro living body imaging system. Maestro imaging system employs the LCTF technique and obtain the image data cube covering spectral range between visual and near infrared light wavelength. The camera pixels number is about 130,000,000. The two modulation range is 420-720 nm and 500-950 nm respectively. A camera obscura is connected with the camera for observation which contain two excitation filters with 50mm and a inside Cermax-type 300W Xenon light sources. One obvious advantage is that it needs no mobile component so that very fine image quality can be guaranteed with no shake, shift and low noise. Thus it is very useful in fluorescent tumor screening, antibody detection, chromosomal localization and angiogenesis labeling.

Rats with tumor region is used to acquire the proper living body hyperspectral fluoroscopic images by Maestro imaging system. A hyperspectral fluoroscopic dataset containing two rats is used in the experiment. Fig. 3 presents the datacute of the dataset, where one rat with tumors in the end of leg is in the left part and a normal rat lies in the right part of Fig. 3. Since the auto fluorescence usually appears similarly with the skins of the rat, it may be difficult to discriminate the signals of tumor fluorescence from the other signals of normal areas. We would introduce the spectral unmixing method in the procedure to do the task.

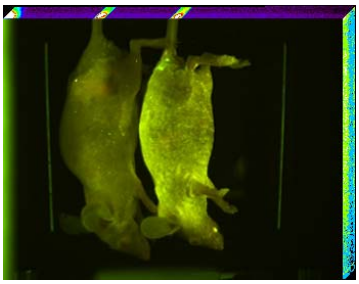

Figure 3. Data cube of the Maestro hyperspectral fluoroscopic images

Fig.4 shows the Quantum dot labeling rats, with the image covering 580-700 nm. C4-2 Prostate cancer cells are xenotransplanted during the three weeks before the experiment. And anti-PSMA anti-body and the excited 640 nm quantum dot are injected two hours before the experiment to label the cancer cells. Since the Quantum excitation spectroscopy covers 600nm – 680nm, the cancer cells' quantum dot signals in the end of the rat's leg obscurely presents red area. However, due to the interference of red fluorescence from the Food chlorophyll and the living body autofluorescence, it becomes impossible to separate the cancer areas by spatial information.

Fig. 4 presents the real positions of the cancer area and the typical areas in the image. It shows that there are autofluorescence areas, which is composed of pure pixels, and a pure pixel refer to one pixel just contain one particular kind material. However, as two the green and purple areas, they are both mixed pixels. One is the mixture of food fluorescence and autofluorescence. Then other is the mixture of autofluorescence and Quantum dot fluorescence. Quantum dot fluorescence is the sign of the existence of cancer cells. The three typical signals or their spectra are shown in Fig. 5. With pure and exact endmembers spectra in hand, it is very easy to get the corresponding abundances maps by least squares methods. However, in practice, prior knowledge about endmembers may be not available before hand in practice. With inaccurate endmembers, many algorithms with the pure pixels assumption would not perform. But it is suitable for NMF, as it needs no pure pixels beforehand. Both endmembers spectra and their corresponding abundances can be automatically extracted by our proposed methods, but our focus lies on the position of them so that the abundances maps are of more importance.

The abundances maps by these different NMF methods are shown in Fig. 6 – Fig. 9. Where it is shown that all the NMF based methods can successfully separate the areas with quantum dot fluorescence, which corresponds to the probable cancer cells. In order to quantitatively compare the proposed method with other state-of-the-art NMF based spectral unmixing algorithms, we obtain the pure endmembers' spectra from the images by some experiential knowledge. Then the spectral angle measure (SAM), spectral information divergence (SID) and the final root-mean-square error (RMSE) by the resulting abundances of these algorithms are shown in Table V. Table V. presents the SAM between the extracted endmembers and the corresponding reference ones, which reveals that our proposed one has the smallest SAM for all the endmembers. It is convincing evidence that our method outperforms the other NMF based methods in generating more accurate endmembers.

Table V. further proves that the corresponding abundances are also more exact so that the reconstruction error by them is lower than those of the other methods. Table shows that compared with the endmembers comparison by SAM, the correspond abundances are even more optimal by our proposed method, since ours presents a much lower RMSE than all the other methods. MVC-MNF constrains the volumn of the simplex constituted by all the possible endmembers so that endmembers are constrained in the NMF solution procedure. MDC-MNF also constrains the endmembers to keep a flat spectral curves. In other words, the endmembers should not contain prominent points in all the corresponding spacetra bands. As to ASC-NMF, it is a classic abundance constrained method, which employs the abundances sum to one constrain to obtain physically meaningful abundances. Above all, compared with the current state-of-the-art two types of constrained NMF, including abundance constraint and endmember constraint, our proposed method performs best. So the spectral dissimilarity constraint proves an promising way to get confidential endmembers' spectra and the corresponding abudances, especially better abundaces.

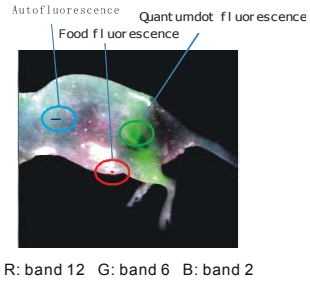

Figure 4. The false color picture of the datacube in our experiments and the most concentrated areas for each fluorescence material

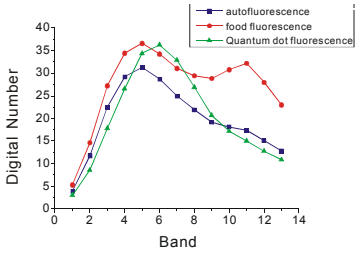

Figure 5. The reference spectra of three materials

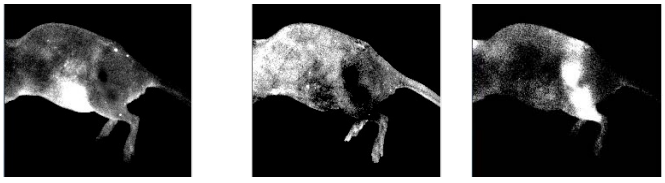

autofluorescence food fluorescence Quantum dot fluorescence

Figure 6. Unmixing results of EDC-MNF

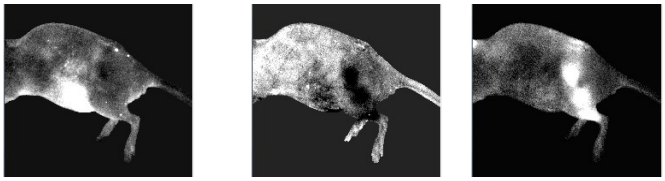

autofluorescence food fluorescence Quantum dot fluorescence

Figure 7. Uunmixing results of MVC-MNF

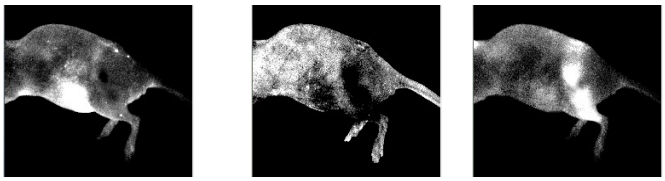

autofluorescence food fluorescence Quantum dot fluorescence

Figure 8. Uunmixing results of MDC-MNF

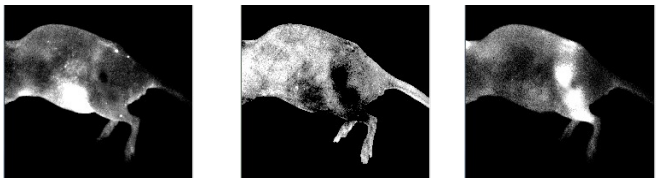

autofluorescence food fluorescence Quantum dot fluorescence

Figure 9. Unmixing results of ASC-NMF

TABLE V. QUANTITATIVE ANALYSIS OF THE RESULTS BY DIFFERENT NMF METHODS

Methods	EDCNMF	MVCNMF	MDCNMF	ASC NMF
SAM	**0.0439**	0.0506	0.0686	0.0453
RMSE	**0.00042**	0.54388	0.00067	0.00178

IV. CONCLUSION

This paper introduces the nonnegative matrix factorization algorithm into fluorescence hyperspectral images processing for cancer screening application. Several state-of-the-art constraints are employed to unmixing hyperspectral images. A novel constraint is also proposed to fully use the dissimilarity of different signals in fluorescence so as to enhance the separability between signals corresponding to the cancer cells and the other interference signals. Both simulated and real fluorescence hyperspectral image datasets are used in our experiments, revealing that: 1) With different levels of noise, our proposed EDC-NMF performs best showing its insensitivity to noise; 2) When the different signals mixing level is high, ours can still get best results, especially the competitive abundances. 3) Combining the autofluorescence imaging with hyperspectral imaging techniques provides a new way to detect probable cancer areas and NMF unmixing methods are promising for this application.

REFERENCES

[1] Wang X, Rosol M, Ge S, et al., "Dynamic tracking of human hematopoietic stem cell engraftment using in vivo bioluminescence imaging," Blood, vol. 102, pp. 3478- 3482, 2003.

[2] Levenson RM, Lynch DT, Kobayashi H et al., “Multiplexing with Multispectral Imaging: From Mice to Microscopy,” ILAR Journal., vol. 49, no. 1, pp.78-88, 2008.

[3] Zhang Y, Han Y, Zhao C L, et al., “Current developments in animal in vivo optical imaging technologies with bioluminescence and fluorescence,” Chinese Bull Life Sci, vol. 18, no.1, pp.25- 30, 2006.

[4] James R. Mansfield, Clifford Hoyt, Richard M. Levenson, “Visualization of Microscopy-Based Spectral Imaging Data from Multi-Label Tissue Sections,” Current Protocols in Molecular Biology, vol. 14, no.19, pp. 1-14, 2008.

[5] Ntziachristos V, Ripoll J, Wang L V, et al. “Looking and listening to light the evolution of whole - body photonic imaging,” NatBiotechnol, vol. 23, no. 3, pp. 313-320, 2005.

[6] S. Harris, R. Wallace, “Acousto-optic tunable filter,” Journal of the Optical Society of America, vol. 59, pp. 744-747, 1969.

[7] S.C. Gebhart, R.C. Thompson, A., “Mahadevan-Jansen, Liquid-crystal tunable filter spectral imaging for brain tumor demarcation,” Applied optics, vol. 46, pp. 1896-1910, 2007.

[8] W. Cai, X. Chen, “Preparation of peptide-conjugated quantum dots for tumor vasculature-targeted imaging,” Nature protocols, vol. 3, pp. 89-96, 2008.

[9] N. Keshava, J.F. Mustard, “Spectral unmixing,” IEEE Signal Processing Magazine, vol. 19, pp. 44-57, 2002.

[10] C.-I Chang, “Hyperspectral Imaging: Techniques for Spectral Detection and Classification,” New York: Plenum, 2003.

[11] N. Keshava, "A survey of spectral unmixing algorithms," Lincoln Laboratory Journal, vol. 14, pp. 55-78, 2003.

[12] D. D. Lee and H. S. Seung, “Algorithms for non-negative matrix factorization,” Adv. Neural Inf. Process. Syst., vol. 13, pp. 556–562, 2000.

[13] S. Moussaoui, H. Hauksdottir, F. Schmidt, C. Jutten, J. Chanussot, D. Brie, S. Doute, and J. A. Benediktsson, “On the decomposition of mars hyperspectral data by ICA and Bayesian positive source separation,” Neurocomputing, vol. 71, no. 10–12, pp. 2194–2208, Jun. 2008.

[14] S. Mika, G. Ratsch, J. Weston, B. Scholkopf, and K. Mullers, "Fisher discriminant analysis with kernels," In Proceedings IEEE Workshop on Neural Networks for Signal Processing, pp. 41-48, 1999.

[15] C. M. Bishop, Pattern recognition and machine learning vol. 4: springer New York, 2006.

[16] I. Jolliffe, Principal component analysis: Wiley Online Library, 2005.

[17] D. Donoho and V. Stodden, When Does Non-Negative Matrix Factorization Give a Correct Decomposition Into Parts, 2003. [online]

[18] Z. Y. Yang, et al., "Blind Spectral Unmixing Based on Sparse Nonnegative Matrix Factorization," IEEE Transactions on Image Processing, vol. 20, pp. 1112-1125, Apr 2011.

[19] A. Huck, et al., "Minimum Dispersion Constrained Nonnegative Matrix Factorization to Unmix Hyperspectral Data," IEEE Transactions on Geoscience and Remote Sensing, vol. 48, pp. 2590-2602, 2010.

[20] L. Miao and H. Qi, “Endmember extraction from highly mixed data using minimum volume constrained nonnegative matrix factorization,” IEEE Transactions on Geoscience and Remote Sensing, vol. 45, no. 3, pp. 765–777, Mar. 2007.

[21] S. Jia and Y. T. Qian, "Constrained Nonnegative Matrix Factorization for Hyperspectral Unmixing," IEEE Transactions on Geoscience and Remote Sensing, vol. 47, pp. 161-173, Jan 2009.

[22] X. S. Liu, et al., "An Approach Based on Constrained Nonnegative Matrix Factorization to Unmix Hyperspectral Data," IEEE Transactions on Geoscience and Remote Sensing, vol. 49, pp. 757-772, Feb 2011.

[23] Pentti Paatero and Unto Tapper. Positive matrix factorization: A non-negative factor model with optimal utilization of error. Environmetrics, vol.5, pp.111-126, 1994.

[24] M. W. Berry, et al., "Algorithms and applications for approximate nonnegative matrix factorization," Computational Statistics & Data Analysis, vol. 52, pp. 155-173, 2007.

[25] C. Deng, et al., "Graph Regularized Nonnegative Matrix Factorization for Data Representation," IEEE Transactions on Pattern Analysis and Machine Intelligence, , vol. 33, pp. 1548-1560, 2011.

[26] N. Y. Guan, et al., "Manifold Regularized Discriminative Nonnegative Matrix Factorization With Fast Gradient Descent," IEEE Transactions on Image Processing, vol. 20, pp. 2030-2048, Jul 2011.

[27] P. O. Hoyer, “Non-negative matrix factorization with sparseness constraints,”J. Mach. Learn. Res., vol. 5, pp. 1457–1469, Dec. 2004.

[28] I. C. Chein, "Spectral information divergence for hyperspectral image analysis," in IEEE Geoscience and Remote Sensing Symposium, vol.1, pp. 509-511, 1999.

[29] A. Plaza, P. Martinez, R. Perez, and J. Plaza, “A quantitative and comparative analysis of endmember extraction algorithms from hyperspectral data,” IEEE Transactions on Geoscience and Remote Sensing, vol. 42, no. 3, pp. 650–663, Mar. 2004.

[30] B .Du, L. Zhang, “Random Selection Based Anomaly Detector for Hyperspectral Imagery,” IEEE Transactions on Geoscience and Remote Sensing, vol. 49, no. 5, pp. 1578 – 1589, May, 2011.

[31] B. Du, L. Zhang., “A Discriminative Manifold Learning Based Dimension Reduction Method for Hyperspectral Classification,” International Journal of Fuzzy Systems, vol. 14, no. 2, pp,272-277,June 2012.